

Small Wideband Coupled-Line Ring Hybrids With No Restriction on Coupling Power

Hee-Ran Ahn, *Senior Member, IEEE*, and Bumman Kim, *Fellow, IEEE*

Abstract—To realize any coupled-line ring hybrid without any restriction on coupling power, a set of coupled-line sections with two shorts was synthesized using one- and two-port equivalent circuits, and design equations were derived to yield perfect matching regardless of the coupling power. Based on the design equations, a new modified Π -type transmission-line equivalent circuit is suggested. It consists mainly of a set of coupled-line sections and can be used to reduce a transmission-line section, especially when the electrical length is greater than 180° . Therefore, the 270° transmission-line section of a conventional ring hybrid can be reduced to less than 90° . To verify the performance of the modified one, two kinds of simulations were performed: in the first, the electrical length of the coupled-line sections was held constant, in the second, the coupling coefficient was held constant. Simulated bandwidths of the resulting small transmission lines depended strongly on coupling power. Using modified and conventional Π -type transmission-line equivalent circuits, a small wideband coupled-line ring hybrid (SWCLRH) was designed. Compared to the conventional ring hybrid, the SWCLRH has much wider bandwidth, but is less than one-third as large. To test the method, a microstrip SWCLRH with a total transmission-line length of 220° was fabricated and tested. Measured S_{21} , S_{41} , S_{23} , and S_{43} were -2.78 , -3.34 , -2.8 , and -3.2 dB, respectively, at a design center frequency of 2 GHz. Matching and isolation with less than -20 dB were achieved in more than 20% fractional bandwidth.

Index Terms—Coupled transmission-line sections with two shorts, modified Π -type transmission-line equivalent circuit, small wideband coupled-line ring hybrids (SWCLRHs), wideband coupled-line ring hybrids (CLRHs).

I. INTRODUCTION

RING HYBRIDS are indispensable and fundamental components that are used for numerous applications including balanced amplifiers, balanced mixers, multipliers, phase shifters and attenuators, power amplifiers, and antenna feeding networks [1]–[3]. However, the conventional ring hybrid, which consists of only transmission-line sections, has inherently narrow bandwidth and large size. To reduce the size, a wideband ring hybrid with a set of coupled-line sections was suggested [4]; in this paper, ring hybrids of this type will be called coupled-line ring hybrids (CLRHs). However, the CLRH can be perfectly

matched only when the coupling coefficient $C = -3$ dB, which cannot be easily realized. To solve this problem, many modifications have been suggested, including using broadside [5] or vertical coupling [6], uniplanar structures [7]–[10], and a left-handed transmission-line section [11]. However, vertical coupling is used only in the form of multisections for wideband performance [6] and the left-handed transmission-line section must be realized using lumped elements. Furthermore, in any case where coupled-line sections are used, -3 -dB coupling cannot be changed for perfect matching [4], [5], [7]–[10].

To attain small ring hybrids, two design methods have been applied: using arbitrary transmission-line sections [7], [12], [13], and using transmission-line equivalent circuits [14], [15], but both methods are unsatisfactory. The small ring hybrids designed by the first method are perfectly matched at frequencies where reduced transmission-line sections become 90° . Therefore, no size reduction effect can be expected. For the second method, lumped-element [16]–[19], Π -type [14], [15] or T-type transmission-line equivalent circuits have been used. However, lumped-element equivalent circuits give very small bandwidths, conventional Π -type equivalent circuits can be used only when the original length of transmission-line sections is less than 180° , and T-type equivalent circuits can achieve size reduction only if the resulting transmission-line section has very high characteristic impedance. Alternative approaches to miniaturizing ring hybrids should be explored.

In this paper, a wideband CLRH is compared with a ring hybrid having a left-handed transmission-line section (LHRH) [11]; the CLRH is better by all criteria. A set of coupled-line sections of the ring hybrid forms a kind of impedance transformer [7], [17] and can be obtained from an impedance-transforming directional coupler [20], [21], but perfect matching can also be achieved only when $C = -3$ dB. To attain perfect matching for any value of C , coupled-line sections with two shorts were synthesized using one- and two-port equivalent circuits, and design equations were derived to fabricate the CLRHs in a planar structure without any restriction on C .

To further reduce the size of ring hybrids, a modified Π -type transmission-line equivalent circuit is also proposed based on the derived design equations of the coupled-line sections with two shorts. The modified equivalent circuit can be used for any transmission-line section whose electrical length is greater than 180° ; therefore, the length of the 270° transmission-line section of a conventional ring hybrid can be reduced. Using both modified and conventional Π -type transmission-line equivalent circuits, a new small wideband coupled-line ring hybrid (SWCLRH) was constructed and compared with a conventional ring hybrid in terms of power division and phase

Manuscript received June 06, 2008; revised November 03, 2008. First published June 12, 2009; current version published July 09, 2009. This work was supported by the Pohang University of Science and Technology (POSTECH) under the BK Program.

The authors are with the Electronic and Electrical Engineering Department, Pohang University of Science and Technology (POSTECH), Pohang, Gyungbuk 790-784, Korea (e-mail: hrahn@postech.ac.kr).

Color versions of one or more of the figures in this paper are available online at <http://ieeexplore.ieee.org>.

Digital Object Identifier 10.1109/TMTT.2009.2022815

responses. Compared to the conventional ring hybrid, the proposed SWCLRH has much wider bandwidth, but is less than one-third as large. To verify the suggested method, one microstrip SWCLRH was fabricated and measured. The measured power divisions S_{21}, S_{41}, S_{23} , and S_{43} were $-2.78, -3.34, -2.8$, and -3.2 dB, respectively, at a design center frequency of 2 GHz; matching and isolation with less than -20 dB were achieved in more than 20% fractional bandwidth.

This paper is organized as follows. Section I provides a brief introduction of conventional wideband ring hybrids and of the contents of this paper. Section II demonstrates that CLRHs are superior to LHRHs by all criteria, but that CLRHs suffer from restriction of coupling power. Section III describes coupled-line sections with two shorts to solve this problem, and suggests wideband CLRHs as an application of the synthesized coupled-line sections with two shorts. Section IV presents methods of further reducing the dimensions of ring hybrids, proposes a modified II-type transmission-line equivalent circuit, and discusses how to obtain SWCLRHs. Section V presents a conclusion.

II. CONVENTIONAL RING HYBRIDS

A. Conventional Ring Hybrids

Three 3-dB conventional ring hybrids terminated in equal impedances Z_0 are depicted in Fig. 1. The conventional ring hybrid in Fig. 1(a) consists of three $\lambda/4$ transmission-line sections and one $3\lambda/4$ transmission-line section and has inherently narrow bandwidth with large size. The main shortcoming of this design is that the bandwidth, where the $\lambda/4$ and $3\lambda/4$ transmission-line sections are 180° out-of-phase, is narrow. Two approaches have been used to increase the bandwidth under this condition. First, in a CLRH, the $3\lambda/4$ transmission-line section is replaced by a set of coupled-line sections with two shorts [see Fig. 1(b)]; in an LHRH, this section is replaced by a left-handed transmission-line section [see Fig. 1(c)]. However, these two ring hybrids have realization problems: in the CLRH, perfect matching can be achieved only when $C = -3$ dB; in the LHRH, the left-handed transmission-line section may be realized only with lumped elements, which may cause unwanted frequency response.

B. Conventional Wideband Ring Hybrids

To compare CLRH and LHRH, the two were simulated at a center frequency of 1 GHz using Advanced Design System (ADS 2006). Even- and odd-mode impedances of the coupled-line sections in Fig. 1(b) were set to 171.4 and 29.3 Ω , respectively, when Z_0 is 50 Ω [4], [5]. The power excited at port ① or ③ (Fig. 1) is divided equally between ports ② and ④ and isolated from port ③ or ①, respectively. The divided waves are in-phase or out-of-phase, depending on which input port is chosen. Considering these points, the ratios of S_{21} to S_{41} and S_{23} to S_{43} , and phase differences of $|\angle S_{21} - \angle S_{41}|$ and $|\angle S_{23} - \angle S_{43}|$ were plotted (Fig. 2) and boundary values were calculated at 100 % fractional bandwidth (Table I).

At 100% fractional bandwidth, S_{21}/S_{41} varied between 0–0.567 dB in the CLRH, and between 0–0.9 dB in the LHRH

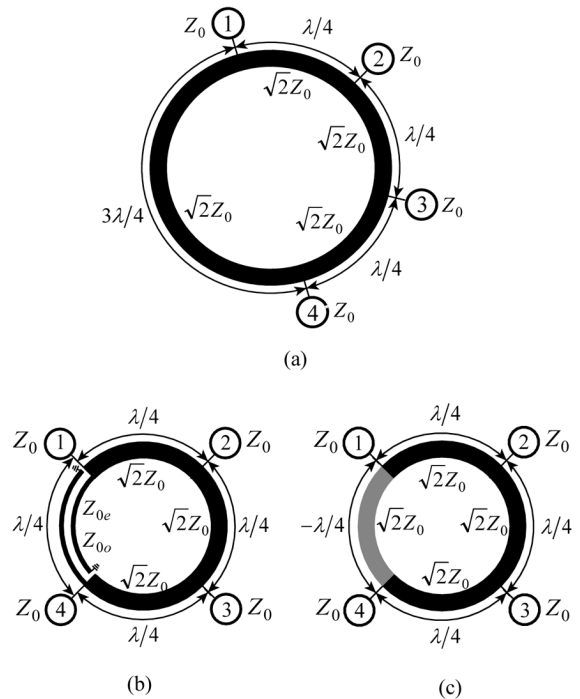


Fig. 1. Conventional ring hybrids. Circled numbers represent ports. (a) Ring hybrid with a $3\lambda/4$ transmission-line section between ports ① and ④. (b) CLRH. (c) Left-handed ring hybrid (LHRH).

[see Fig. 2(a)]; S_{23}/S_{43} varied between 0–0.724 dB in the CLRH and between -0.9 –0 dB in the LHRH [see Fig. 2(b)]. Smaller power ratios are desirable; therefore, the CLRH is better than the LHRH by this criterion.

The phase responses of the CLRH and LHRH differed. The out-of-phase response $|\angle S_{21} - \angle S_{41}|$ is between 170.4° – 188.3° in the CLRH and between 137.6° – 228.3° in the LHRH [see Fig. 2(c)]. The in-phase response $|\angle S_{23} - \angle S_{43}|$ is between 0° – 9.4° in the CLRH and between 0° – 25.66° in the LHRH [see Fig. 2(d)]. since the ideal phase difference is 180° for $|\angle S_{21} - \angle S_{41}|$ and 0° for $|\angle S_{23} - \angle S_{43}|$, the CLRH has much better phase response than the LHRH. Therefore, CLRH are also superior to LHRH by this criterion.

Although the performance of the CLRH is better than that of the LHRH, realizing the simulated values of 171.4- Ω high even-mode impedance and 29.3- Ω low odd-mode impedance in microstrip technology is very difficult. To identify ways to solve this problem, the coupled-line sections with two shorts connected between ports ① and ④ [see Fig. 1(b)] will be discussed in more detail.

III. COUPLED-LINE SECTIONS WITH TWO SHORTS AND THEIR APPLICATION TO WIDEBAND RING HYBRIDS

A. Coupled-Line Sections With Two Shorts

Coupled-line sections with two shorts connected between ports ① and ④ [see Fig. 1(b)] are used as an impedance transformer to transform $2Z_0$ into Z_0 when power is fed into port ① [7], [17]. An impedance-transforming directional coupler [see Fig. 3(a)] may be used to create an impedance-transforming coupled-line section with two shorts [see Fig. 3(b)] [20], [21].

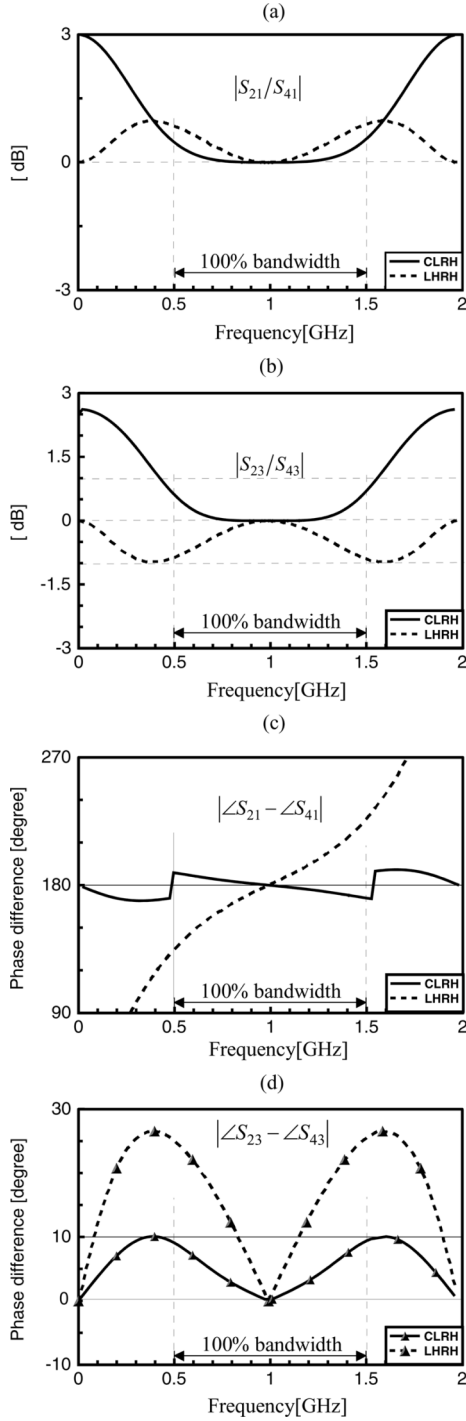


Fig. 2. Simulated frequency responses of the CLRH and LHRH. (a) Divided power ratio of $|S_{21}/S_{41}|$. (b) Divided power ratio of $|S_{23}/S_{43}|$. (c) Out-of-phase response of $|\angle S_{21} - \angle S_{41}|$. (d) In-phase response of $|\angle S_{23} - \angle S_{43}|$. Solid lines: CLRH. Dotted lines: LHRH.

TABLE I
SIMULATION RESULTS AT 100% FRACTIONAL BANDWIDTH

Parameter	CLRH	LHRH
(S_{21}/S_{41}) [dB]	0 ~ 0.567	0 ~ 0.902
(S_{23}/S_{43}) [dB]	0 ~ 0.724	-0.902 ~ 0
$ \angle S_{21} - \angle S_{41} $ [°]	170.4 ~ 188.3	137.6 ~ 228.3
$ \angle S_{23} - \angle S_{43} $ [°]	0 ~ 9.4	0 ~ 25.66

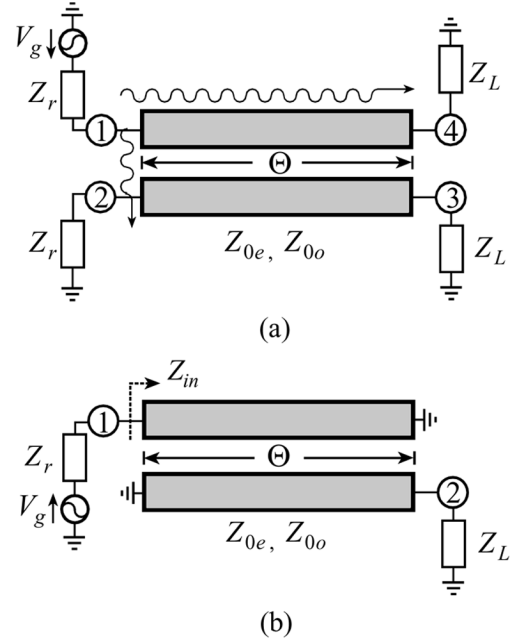


Fig. 3. Impedance-transforming directional coupler and a set of coupled-line sections with two shorts. (a) Directional coupler. (b) Set of coupled-line sections with two shorts, marking input impedance Z_{in} looking into the coupled-line sections terminated in Z_L at port ②.

When $\Theta = 90^\circ$ [see Fig. 3(a)], the power excited at port ① is coupled to port ② with a certain coupling power and the remainder of the input power is delivered to port ④. Theoretically, no power is delivered to port ③, which is called an isolated port. In this case, the even-mode impedance Z_{0e} and odd-mode impedance Z_{0o} [20], [21] are

$$Z_{0e} = \sqrt{Z_r Z_L} \sqrt{\frac{1+C}{1-C}} \quad (1a)$$

$$Z_{0o} = \sqrt{Z_r Z_L} \sqrt{\frac{1-C}{1+C}}. \quad (1b)$$

Terminating ports ② and ④ in Fig. 3(a) in shorts results in the coupled-line sections with shorts in Fig. 3(b). Applying the short boundary condition gives the admittance matrix Y of the circuit in Fig. 3(b) as

$$Y = \begin{bmatrix} -j \frac{Y_{0e} + Y_{0o}}{2} \cot \Theta & -j \frac{Y_{0o} - Y_{0e}}{2} \csc \Theta \\ -j \frac{Y_{0o} - Y_{0e}}{2} \csc \Theta & -j \frac{Y_{0e} + Y_{0o}}{2} \cot \Theta \end{bmatrix}. \quad (2)$$

Based on Y , the scattering parameters of coupled-line sections [see Fig. 3(b)] are derived as (Appendix)

$$S_{11} = \frac{1}{D} [(Y_{0o} - Y_{0e})^2 \sec^2 \Theta - (Y_{0e} + Y_{0o})^2 - 4Y_r Y_L \tan^2 \Theta - j2(Y_{0o} + Y_{0e}) \times (Y_L - Y_r) \tan \Theta] \quad (3a)$$

$$S_{22} = \frac{1}{D} [(Y_{0o} - Y_{0e})^2 \sec^2 \Theta - (Y_{0e} + Y_{0o})^2 - 4Y_r Y_L \tan^2 \Theta + j2(Y_{0o} + Y_{0e}) \times (Y_L - Y_r) \tan \Theta] \quad (3b)$$

$$S_{21} = \frac{1}{D} [-j4Y_r(Y_{0o} - Y_{0e}) \sin \Theta \sec^2 \Theta] \quad (3c)$$

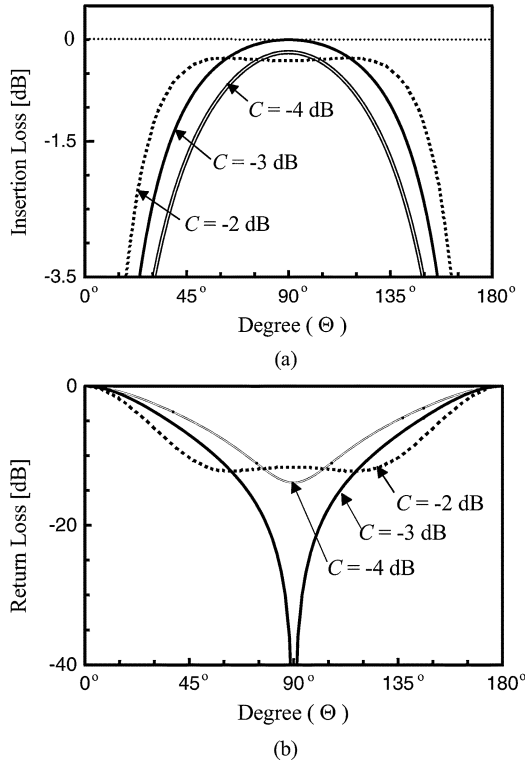


Fig. 4. Simulation results of the coupled-line sections with two shorts for different C . (a) Insertion loss. (b) Return loss (matching).

where $D = (Y_{0e} + Y_{0o})^2 - (Y_{0o} - Y_{0e})^2 \sec^2 \Theta - 4Y_r Y_L \tan^2 \Theta + j2(Y_{0e} + Y_{0o})(Y_r + Y_L) \tan \Theta$, $Y_r = 1/Z_r$, and $Y_L = 1/Z_L$.

Using the scattering parameters calculated in (3), the coupled-line sections with two shorts were simulated using MATLAB 6.1 (The MathWorks Inc., Natick, MA) for termination impedances $Z_r = 50 \Omega$ and $Z_L = 100 \Omega$. In Fig. 4, depending on C , coupling characteristics are classified as critical coupling ($C = -3$ dB), over-coupling ($C > -3$ dB), and under-coupling ($C < -3$ dB) [22]. Only critical coupling gives no insertion loss and perfect matching, and over-coupling results in ripples with no perfect matching (Fig. 4). The power excited at port ① [see Fig. 3(b)] is transmitted to port ②, and the amount of transmitted power depends on the coupling structure. To achieve perfect matching at a design center frequency regardless of C , design equations given in (1) should be modified. This modification process and the resulting design equations will be explained in more detail using one- and two-port equivalent circuits.

B. One-Port Equivalent Parallel Resonant Circuit

How much power excited at port ① [see Fig. 3(b)] that can be transmitted into port ② depends on the coupling structure. Therefore, the coupled-line sections terminated in Z_L in Fig. 3(b) may be equivalent to a one-port parallel resonant circuit [22], as described in Fig. 5, where input impedance and input reference impedance Z_{in} and Z_r are indicated. The input impedance Z_{in} [23] was calculated as follows:

$$Z_{in} = [Y_{in}]^{-1} = \left[Y_{11} - \frac{Y_{12}Y_{21}}{Y_{22} + Y_L} \right]^{-1} \quad (4)$$

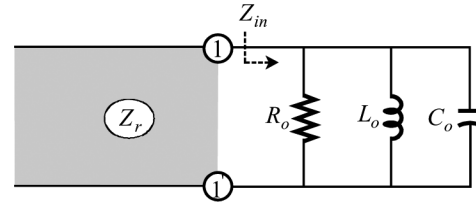


Fig. 5. One-port equivalent parallel resonant circuit. Input impedance Z_{in} ; input reference impedance Z_r .

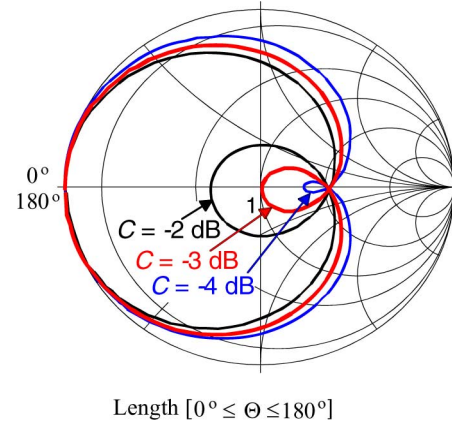


Fig. 6. Input impedances are illustrated on an impedance Smith chart depending on over, critical, and under coupling.

which gives frequency-dependent R_o , L_o and C_o (Fig. 5) as (see the Appendix)

$$R_o = \frac{Y_L(1 - C^2) + Y_r \cot^2 \Theta}{Y_r Y_L C^2 \csc^2 \Theta}. \quad (5a)$$

Values of L_o and C_o depend on Θ . For $\cot \Theta \geq 0$,

$$\omega C_o = C^2 \left[\sqrt{\frac{Y_r Y_L}{1 - C^2}} \right]^3 \frac{\cot \Theta}{\sin^2 \Theta} \quad (5b)$$

$$\omega L_o = \frac{(\sqrt{1 - C^2})^3}{Y_L \sqrt{Y_r Y_L} \cot \Theta [Y_r \cot^2 \Theta + Y_L(1 - C^2)]} \quad (5c)$$

For $\cot \Theta < 0$,

$$\omega C_o = \frac{Y_L \sqrt{Y_r Y_L} \cot \Theta [Y_r \cot^2 \Theta + Y_L(1 - C^2)]}{(\sqrt{1 - C^2})^3} \quad (5d)$$

$$\omega L_o = \left[\sqrt{\frac{1 - C^2}{Y_r Y_L}} \right]^3 \frac{\sin^2 \Theta}{C^2 \cot \Theta}. \quad (5e)$$

The input impedance Z_{in} may be displayed on an impedance Smith chart. The three loci in Fig. 6 show the input impedances normalized to Z_r when $Z_r = 50 \Omega$ and $Z_L = 100 \Omega$ are fixed, and C and electrical length Θ are varied [see Fig. 3(b)]. Each locus cuts the real axis twice, and when $\Theta = 90^\circ$, the value is exactly unity with the critical coupling, but more or less than unity with two other couplings. This means that perfect matching occurs only under the condition of critical coupling; these results agree with those in Fig. 4. For any set of coupled-line sections with two shorts [see Fig. 3(b)] to have perfect matching regardless of C , conventional even- and odd-mode impedances in (1) must be modified to increase over-coupled input impedances and decrease under-coupled input impedances.

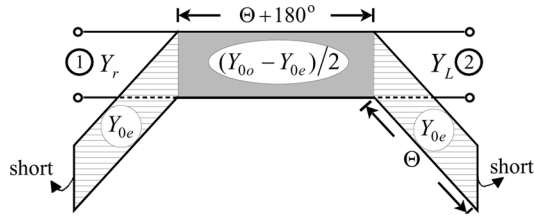


Fig. 7. Two-port equivalent circuit of coupled-line sections with two shorts.

When $\Theta = 90^\circ$ in (5), only R_o appears and its value is

$$R_o = Z_r \frac{1 - C^2}{C^2}. \quad (6)$$

From (6), $R_o = Z_r$ when $C = 1/\sqrt{2}$ (critical coupling), which agrees with the simulation results (Figs. 4 and 6). To perfectly match coupled-line sections at a design center frequency at any C , the even- and odd-mode impedances should be modified so that $R_o = Z_r$ always, regardless of C . Z_r in (6) comes from the even- and odd-mode impedances in (1) and can be modified to have a constant value of input impedance by replacing Z_r in (1) with $Z_r[C^2/(1 - C^2)]$. In this way, the modified even- and odd-mode impedances Z_{0e}^m and Z_{0o}^m are derived as

$$Z_{0e}^m = \frac{C}{1 - C} \sqrt{Z_r Z_L} \quad (7a)$$

$$Z_{0o}^m = \frac{C}{1 + C} \sqrt{Z_r Z_L}. \quad (7b)$$

With Z_{0e}^m and Z_{0o}^m , the input impedance Z_{in} always becomes $R_o = Z_r$ at resonant frequency, i.e., at a center frequency, regardless of C .

C. Two-Port Equivalent Circuit

A set of coupled-line sections with electrical length Θ and termination admittances Y_r and Y_L [see Fig. 3(b)] may be equivalent to a circuit that consists of a transmission-line section with electrical length $\Theta + 180^\circ$ and two short stubs (Fig. 7) where the characteristic admittances are $(Y_{0o} - Y_{0e})/2$ for the transmission-line section and Y_{0e} for the short stubs. When $\Theta = 90^\circ$, only the transmission-line section connects the two termination admittances; thus, this section becomes an admittance transformer. Therefore, its characteristic admittance is the geometric mean of the two termination admittances and is also related to C [20], [21]. Thus, the relative relations are given as

$$\frac{Y_{0o} - Y_{0e}}{2} = \sqrt{Y_r Y_L} \quad (8a)$$

$$Y_{0o} = \frac{1 + C}{1 - C} Y_{0e}. \quad (8b)$$

The even- and odd-mode admittances satisfying (8) are different from those in (1) and are calculated as

$$Y_{0e}^m = \frac{1 - C}{C} \sqrt{Y_r Y_L} \quad (9a)$$

$$Y_{0o}^m = \frac{1 + C}{C} \sqrt{Y_r Y_L} \quad (9b)$$

which are the same as those in (7).

In the equivalent circuit (Fig. 7), the transmission-line section can be considered as a circuit in which a transmission-line

TABLE II
MODIFIED EVEN- AND ODD-MODE IMPEDANCES WITH
 $Z_r = 100 \Omega$ AND $Z_L = 50 \Omega$ [SEE FIG. 3(b)]

C	-3 dB	-5 dB	-7 dB	-9 dB	-11 dB
Z_{0e}^m [Ω]	171.4	90.9	57.1	38.9	27.8
Z_{0o}^m [Ω]	29.3	25.5	21.8	18.5	15.5

section with electrical length Θ is connected to a frequency-independent 180° phase shifter. Therefore, the $\lambda/4$ transmission-line section and $\lambda/4$ coupled-line sections [see Fig. 1(b)] can be 180° out-of-phase in a wider frequency band. This is the reason the CLRH [see Fig. 1(b)] can have wideband performance.

D. Coupled-Line Section Measurements

To verify the design equations in (7) and (9), a microstrip coupled-line section with two shorts terminated in 100 and 50 Ω was fabricated on a substrate with thickness $H = 0.76$ mm and relative permittivity $\epsilon_r = 3.4$, and tested at a center frequency of 2 GHz. Z_{0e}^m and Z_{0o}^m both decreased with C (Table II). At $C = -3$ dB (i.e., the value required to attain critical coupling), the even-mode impedance was 171.4 Ω and the odd-mode impedance was 29.3 Ω ; these values are almost impossible to realize with 2-D microstrip lines. For measurement, a set of coupled-line sections with $C = -7$ dB was fabricated; its even-mode impedance was $Z_{0e}^m = 57.1 \Omega$ and its odd-mode impedance was $Z_{0o}^m = 21.8 \Omega$ (Table II).

$Z_{0e}^m = 57.1 \Omega$ and $Z_{0o}^m = 21.8 \Omega$ required above can be realized easily using printed circuit board (PCB) technology, but an easier method of attaining the odd-mode impedance will be introduced in the following paragraphs. The even-mode impedance of 57.1 Ω can be realized easily, but realizing the odd-mode impedance of 21.8 Ω is more difficult with the given substrate. Therefore, a 3-D structure or a set of three coupled-line sections is needed to attain such a low odd-mode impedance. In our case, a 3-D structure [24] was used.

If a TEM propagation of two coupled transmission lines is assumed, then the characteristics of coupled transmission lines can be completely determined from capacitances and propagation velocities on the transmission lines. A 2-D capacitance equivalent network of a pair of coupled transmission lines was depicted in Fig. 8(a). In this case, C_{12} is the capacitance per unit length between the two conductor lines in the absence of the ground conductor, while C_{11} and C_{22} are the capacitances per unit length between one conductor and ground in the absence of the other conductor line. If the coupled transmission lines are identical in size, $C_{11} = C_{22}$. For even-mode excitation, no current flows between the two transmission lines; therefore, the capacitance C_{12} per unit length between the two conductor lines is 0 in the absence of the ground conductor. Therefore, the resulting capacitance of either line to ground is $C_e = C_{11} = C_{22}$ and its even-mode impedance Z_{0e} is $\sqrt{\epsilon\mu}/C_e$, where ϵ and μ are a substrate's permittivity and permeability. For the odd-mode excitation, the electric field lines have an odd symmetry about the center line and a voltage null exists between the two transmission lines. Therefore, the resulting capacitance of either line to ground is $C_o = C_{11} + 2C_{12}$ and the odd-mode impedance

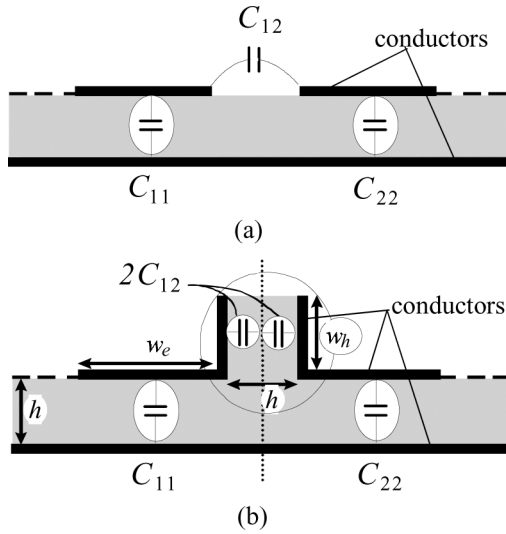


Fig. 8. General TEM coupled lines. (a) Side view of a 2-D equivalent capacitance network. (b) Side view of a 3-D equivalent capacitance network.

Z_{0o} is $\sqrt{\varepsilon\mu}/C_o$. The even- and odd-mode impedances are proportional to $\sqrt{\varepsilon}$ so if the odd-mode capacitance is too high, i.e., if coupling is tight, the odd-mode impedance is not easy to realize.

To realize the low odd-mode impedance with a 3-D structure, as in Fig. 8(b), a pair of coupled-line sections, with which only the required even-mode impedance can be realized, was first fabricated with a space of h . Here, h is an assumed thickness of a given substrate. The width w_h [see Fig. 8(b)] of a vertically constructed conductor is then determined to have the required odd-mode impedance. In this case, the even-mode impedance is connected in parallel with the impedance produced by the vertical conductor.

For the given substrate, a pair of coupled transmission lines was first realized, fixing its space at the thickness of the substrate so that only the even-mode impedance of 57.1Ω can be obtained. For the odd-mode excitation, a voltage null exists between two coupled transmission lines so the even-mode impedance of 57.1Ω was connected in parallel with the impedance produced between a vertically constructed conductor and the voltage null between the two coupled lines. This resulted in the required odd-mode impedance $Z_{0o}^m = 21.8 \Omega$. Therefore, the impedance Z_v produced by the vertical conductor is 35.3Ω . The characteristic impedance Z_v is easily realized using any commercial circuit simulation tool, but an important point is that its effective thickness is half of the given substrate thickness. Microstrip-coupled transmission-line sections were fabricated [see Fig. 9(a)] using appropriate design parameters (Table III). Measured and predicted results agree well [see Fig. 9(b)].

E. Application to Wideband CLRHs

Using the analyzed coupled lines, wideband CLRHs can be realized without any restriction on C . A set of coupled-line sections between ports ① and ④ [see Fig. 1(b)] is a kind of impedance transformer that transforms $100\text{--}50 \Omega$ when $Z_0 = 50 \Omega$. Therefore, the data in Table II were used and excitation at port ① was compared for several CLRHs (Fig. 10). Perfect power divisions [see Fig. 10(a) and (b)] perfect isolation [see

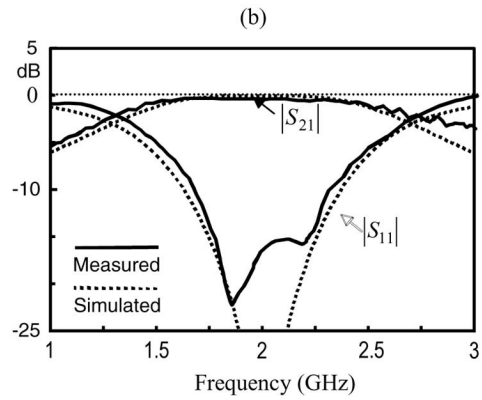
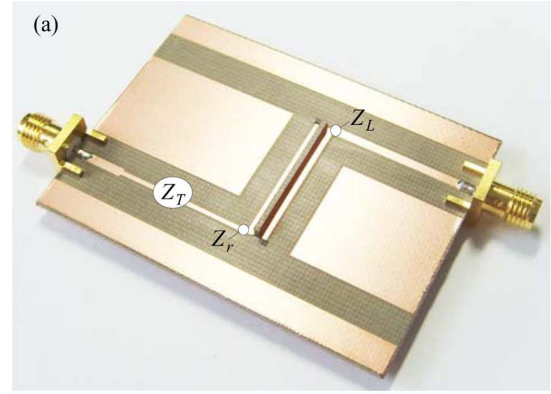


Fig. 9. Set of coupled transmission-line sections with two different termination impedances. (a) Fabricated coupled transmission-line sections. (b) Results measured and simulated are compared.

TABLE III
FABRICATION DATA FOR A SET OF MICROSTRIP
COUPLED-LINE SECTIONS WITH TWO SHORTS

$Z_r = 100 \Omega$, $Z_L = 50 \Omega$, $Z_T = 70.71 \Omega$	
$Z_{0e}^m = 57.1 \Omega$	$w_e = 1.34 \text{ mm}$, $\ell = 22.9 \text{ mm}$, $s = 0.76 \text{ mm}$
$Z_{0o}^m = 21.8 \Omega$	$Z_v = 35.3 \Omega \rightarrow w_h = 1.407 \text{ mm}$, $\ell = 22.9 \text{ mm}$
$Z_T = 70.71 \Omega$	$w = 0.895 \text{ mm}$, $\ell = 23.28 \text{ mm}$
50Ω	$w = 1.678 \text{ mm}$

s : gap between two transmission-line sections,
 ℓ : physical length of transmission-line sections

Fig. 10(c)], and perfect matching [see Fig. 10(d)] at a center frequency of 1 GHz were achieved regardless of C , and the bandwidth was proportional to the coupling power.

IV. SWCLRHs

A. Small Transmission Lines

The CLRHs and LHRHs [see Fig. 1(b) and (c)] are somewhat smaller than the conventional ring hybrids [see Fig. 1(a)], but they are still large. To further reduce the size of ring hybrids, transmission-line sections must be reduced. For this purpose, a conventional Π -type transmission-line equivalent circuit

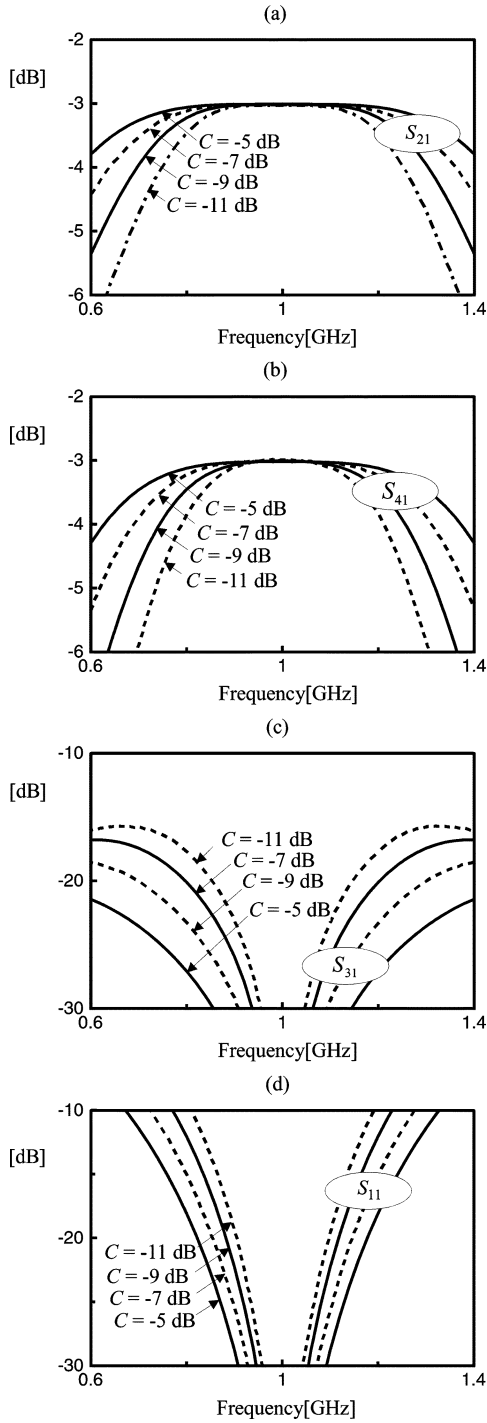


Fig. 10. Several CLRHs. (a) Power division (S_{21}). (b) Power division (S_{41}). (c) Isolation (S_{31}). (d) Matching (S_{11}).

has been suggested [14], but it can be used only when its electrical length is less than 180° . To further reduce the size of ring hybrids, a modified Π -type transmission-line equivalent circuit is suggested here. It can be used to reduce the $3\lambda/4$ transmission-line section of a conventional ring hybrid to less than 90° .

Several transmission-line sections with characteristic impedance Z_0 can be designed for $\Theta < 180^\circ$ and $\Theta_s < 90^\circ$ (e.g., Fig. 11). The equivalent circuit consisting of a transmission-line section [see Fig. 11(b)] is used when its original total electrical length is less than 180° and that consisting of coupled-line sections [see Fig. 11(d)] is used when it is more than 180° .

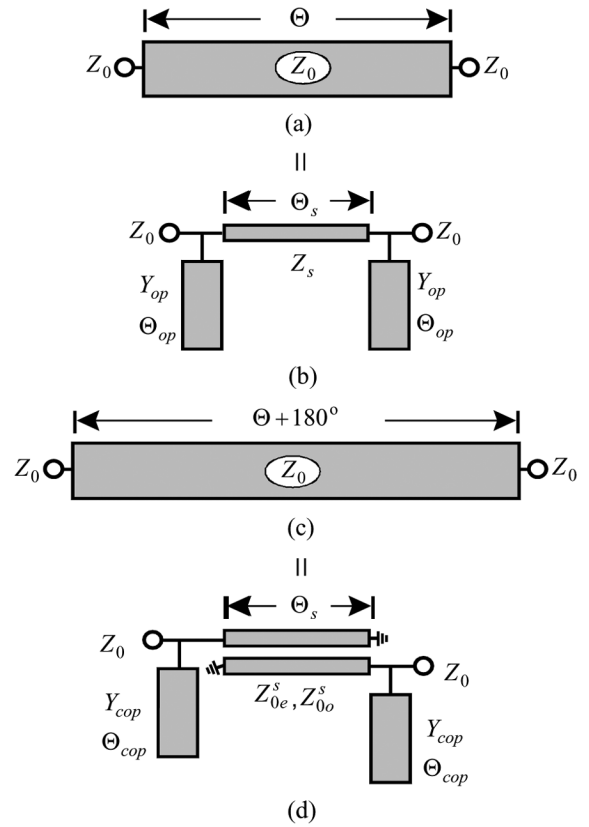


Fig. 11. Transmission-line sections and their equivalent circuits. (a) Transmission-line section with $\Theta \leq 180^\circ$. (b) Conventional Π -type transmission-line equivalent circuit with $\Theta_s \leq 90^\circ$. (c) Transmission-line section with $0^\circ \leq \Theta < 180^\circ$. (d) Modified Π -type transmission-line equivalent circuit with $\Theta_s \leq 90^\circ$.

The even- and odd-mode impedances Z_{0e}^s and Z_{0o}^s [see Fig. 11(d)] were computed, applying $Z_r = Z_L$ [see Fig. 3(b)] in (7) and (9). The relationships between Θ , Z_0 , Z_s , Θ_s , Y_{op} , Θ_{op} , Z_{0e}^s , Z_{0o}^s , Y_{cop} , and Θ_{cop} (Fig. 11) can be derived as

$$Z_s = Z_0 \frac{\sin \Theta}{\sin \Theta_s} \quad (10a)$$

$$Y_{op} \tan \Theta_{op} = Y_0 \frac{\cos \Theta_s - \cos \Theta}{\sin \Theta} \quad (10b)$$

$$Z_{0e}^s = Z_0 \frac{\sin \Theta}{\sin \Theta_s} \frac{C}{1 - C} \quad (11a)$$

$$Z_{0o}^s = Z_0 \frac{\sin \Theta}{\sin \Theta_s} \frac{C}{1 + C} \quad (11b)$$

$$Y_{cop} \tan \Theta_{cop} = \frac{Y_0}{\sin \Theta} \left(\frac{\cos \Theta_s - C \cos \Theta}{C} \right) \quad (11c)$$

where $Y_0 = 1/Z_0$.

When $Z_0 = 70.71 \Omega$ and $\Theta = 90^\circ$ [see Fig. 11(c)], the circuit is equal to the $3\lambda/4$ transmission-line section between ports ① and ④ of the conventional ring hybrid [see Fig. 1(a)]. Based on (10) and (11), Z_{0e}^s , Z_{0o}^s , and Z_{cop} were calculated while varying C for fixed values $\Theta_s = 60^\circ$, $Z_0 = 70.71 \Omega$, $\Theta = 90^\circ$, $\Theta_{cop} = 30^\circ$ (Table IV). Similarly, Z_{0e}^s , Z_{0o}^s , and Z_{cop} were calculated while varying Θ_s for fixed values $C = -7 \text{ dB}$, $Z_0 = 70.71 \Omega$, $\Theta = 90^\circ$, and $\Theta_{cop} = 30^\circ$ (Table V). Using these calculated values, several small transmission-line sections [see

TABLE IV
DESIGN DATA FOR SMALL TRANSMISSION LINES
WITH A FIXED VALUE $\Theta_s = 60^\circ$

$\Theta_s = 60^\circ,$ $Z_0 = 70.71 \Omega, \Theta = 90^\circ, \Theta_{cop} = 30^\circ$			
C [dB]	-5	-7	-9
Z_{0e}^s	104.9	65.9	44.9
Z_{0o}^s	29.4	25.2	21.4
Z_{cop}	45.9	36.5	29

TABLE V
DESIGN DATA FOR SMALL TRANSMISSION LINES
WITH A FIXED VALUE $C = -7$ dB

$C = -7$ dB, $Z_0 = 70.71 \Omega, \Theta = 90^\circ, \Theta_{cop} = 30^\circ$			
Θ_s	40°	50°	60°
Z_{0e}^s	88.8	74.5	65.9
Z_{0o}^s	33.97	28.5	25.2
Z_{cop}	23.8	28.4	36.5

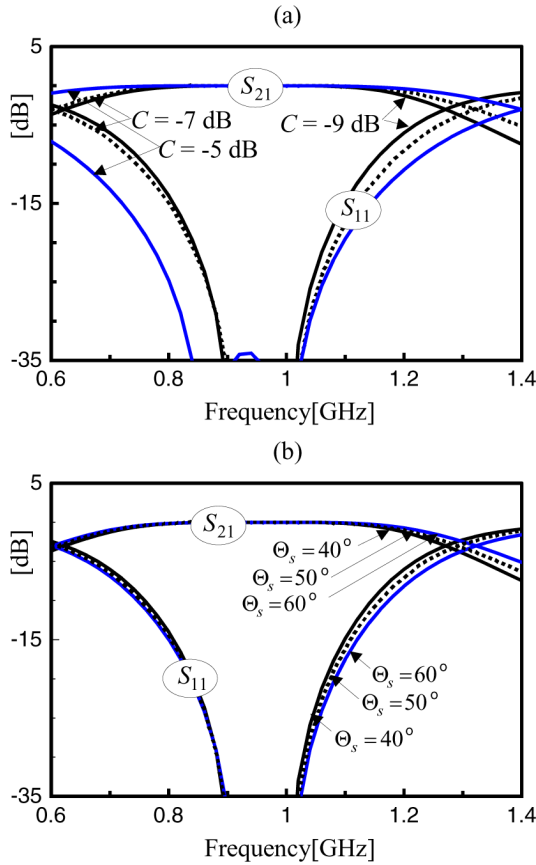


Fig. 12. Simulation results of small transmission-line sections shown in Fig. 11(d). (a) Θ_s is fixed at 60° and coupling coefficients are varied. (b) Coupling coefficient C is fixed at -7 dB and Θ_s is varied.

Fig. 11(d)] were simulated. Greater coupling power gives more bandwidth [see Fig. 12(a)], but the bandwidth is not strongly dependent on the electrical length Θ_s if C is fixed [see Fig. 12(b)].

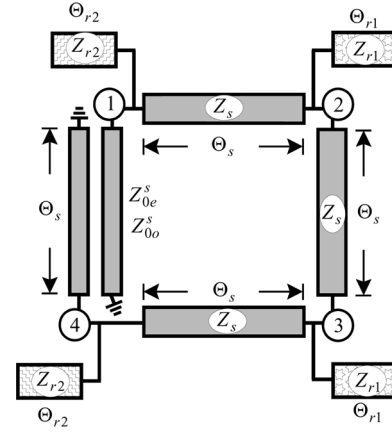


Fig. 13. Proposed SWCLRH.

TABLE VI
DESIGN DATA OF SMALL WIDEBAND COUPLED-LINE
RING HYBRIDS FOR $\Theta_s = 40^\circ$

$\Theta_s = 40^\circ$				
$Z_s = 110 \Omega, Z_{r1} = 38.73 \Omega, \Theta_{r1} = 40^\circ$				
C	-3 dB	-5 dB	-7 dB	-9 dB
Z_{0e}^s	266.7 Ω	141.3 Ω	88.8 Ω	60.5 Ω
Z_{0o}^s	45.6 Ω	39.6 Ω	33.97 Ω	28.8 Ω
Z_{r2}	32.1 Ω	27.9 Ω	23.9 Ω	20.3 Ω
Θ_{r2}	40°	40°	40°	40°

TABLE VII
DESIGN DATA OF SMALL WIDEBAND COUPLED-LINE
RING HYBRIDS FOR $\Theta_s = 50^\circ$

$\Theta_s = 50^\circ$				
$Z_s = 92.3 \Omega, Z_{r1} = 65.5 \Omega, \Theta_{r1} = 50^\circ$				
C	-3 dB	-5 dB	-7 dB	-9 dB
Z_{0e}^s	223.7 Ω	118.6 Ω	74.5 Ω	50.8 Ω
Z_{0o}^s	38.2 Ω	33.2 Ω	28.5 Ω	24.2 Ω
Z_{r2}	54.3 Ω	47.2 Ω	40.5 Ω	34.3 Ω
Θ_{r2}	50°	50°	50°	50°

TABLE VIII
DESIGN DATA OF SMALL WIDEBAND COUPLED-LINE
RING HYBRIDS FOR $\Theta_s = 60^\circ$

$\Theta_s = 60^\circ$				
$Z_s = 81.6 \Omega, Z_{r1} = 59.3 \Omega, \Theta_{r1} = 40^\circ$				
C	-3 dB	-5 dB	-7 dB	-9 dB
Z_{0e}^s	197.9 Ω	104.9 Ω	65.9 Ω	44.9 Ω
Z_{0o}^s	33.8 Ω	29.4 Ω	25.2 Ω	21.4 Ω
Z_{r2}	69.8 Ω	60.7 Ω	52.0 Ω	44.1 Ω
Θ_{r2}	50°	50°	50°	50°

B. SWCLRHS

Using the established relationships (Fig. 11), an SWCLRH was fabricated (Fig. 13) in which the following relations hold:

$$Y_{r1} \tan \Theta_{r1} = 2Y_{op} \tan \Theta_{op} \quad (12a)$$

$$Y_{r2} \tan \Theta_{r2} = Y_{op} \tan \Theta_{op} + Y_{cop} \tan \Theta_{cop} \quad (12b)$$

where $Y_{r1} = 1/Z_{r1}$ and $Y_{r2} = 1/Z_{r2}$.

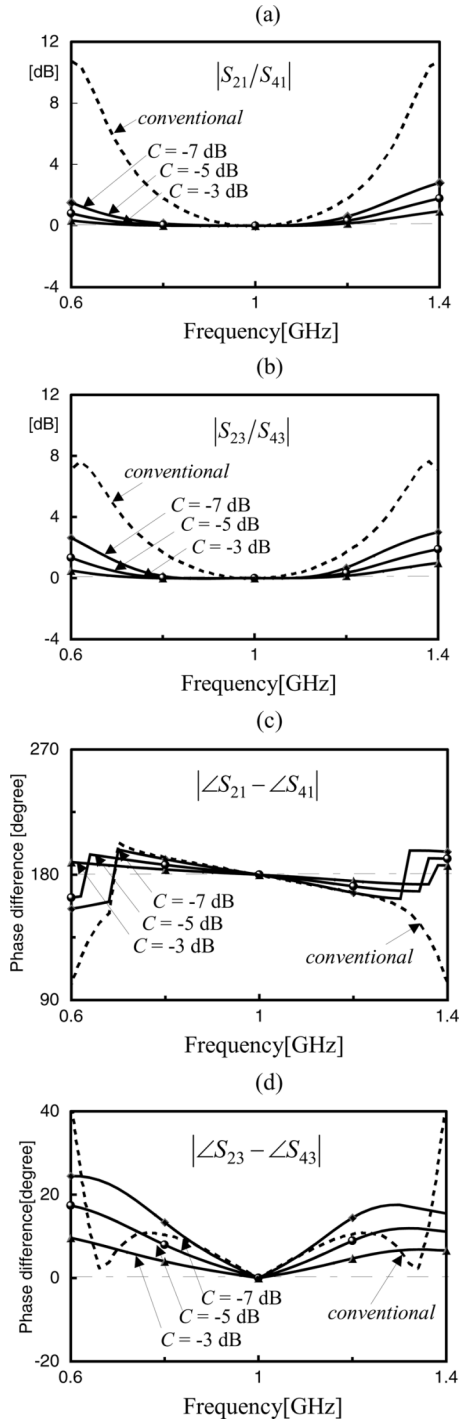


Fig. 14. SWCLRHRs are compared with a conventional ring hybrid. (a) Divided power ratio of $|S_{21}/S_{41}|$. (b) Divided power ratio of $|S_{23}/S_{43}|$. (c) Out-of-phase response of $|\angle S_{21} - \angle S_{41}|$. (d) In-phase response of $|\angle S_{23} - \angle S_{43}|$.

The SWCLRHRs were designed using (10)–(12) and three types of data with variable Θ_s were calculated where Θ_s , Θ_{r1} , and Θ_{r2} were fixed and C was varied from -3 to -9 dB in increments of -2 dB (Tables VI–VIII). Using Table VI, the SWCLRHRs were designed at a center frequency of 1 GHz and simulation power ratios [see Fig. 14(a) and (b)] and phase differences [see Fig. 14(c) and (d)] were compared to those of a conventional ring hybrid. The total transmission-line length of the SWCLRHR is 160° , whereas that of the conventional

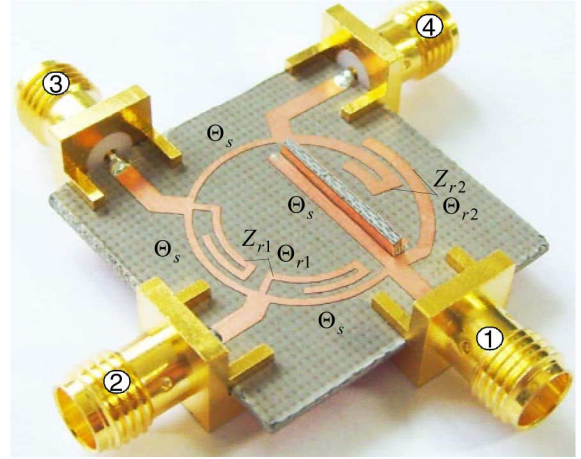


Fig. 15. Fabricated microstrip small ring hybrid.

TABLE IX
FABRICATION DATA FOR A MICROSTRIP SMALL
WIDEBAND CLRH

$\Theta_s = 55^\circ$, $Z_s = 86.3 \Omega$, $Z_{0e}^s = 64.21 \Omega$, $Z_{0o}^s = 25.8 \Omega$	
$(Z_{r1} = 86.4 \Omega, \Theta_{r1} = 54.5^\circ)$,	
$(Z_{r2} = 63.85 \Omega, \Theta_{r2} = 60^\circ)$	
$Z_s = 86.3 \Omega$	$w = 0.58 \text{ mm}$, $\ell = 14.5 \text{ mm}$
$Z_{0e}^s = 64.21 \Omega$	$w_e = 1.08 \text{ mm}$, $\ell = 13.8 \text{ mm}$, $s = 0.76 \text{ mm}$
$Z_{0o}^s = 25.8 \Omega$	$Z_v = 43.16 \Omega \rightarrow$ $w_h = 1.04 \text{ mm}$, $\ell = 13.8 \text{ mm}$
(Z_{r1}, Θ_{r1})	$w = 0.577 \text{ mm}$, $\ell = 14.32 \text{ mm}$
(Z_{r2}, Θ_{r2})	$w = 1.08 \text{ mm}$, $\ell = 15.4 \text{ mm}$
50Ω	$w = 1.687 \text{ mm}$

s : gap between two transmission-line sections,
 ℓ : physical length of transmission-line sections.

one is 540° . The proposed SWCLRHR shows wider bandwidth than the conventional ring hybrid, as demonstrated in Fig. 14, despite being less than one-third its size.

C. SWCLRHR Measurement

To verify the design method, one microstrip SWCLRHR was fabricated on a substrate ($H = 0.76 \text{ mm}$ and $\epsilon_r = 3.4$) (Fig. 15). Fabrication data (Table IX) were collected with the transmission-line section Θ_s fixed at 55° , Z_{0e}^s set to 64.21Ω and Z_{0o}^s set to 25.8Ω . The microstrip SWCLRHR was tested at a center frequency of 2 GHz and the measured and predicted results were compared (Fig. 16).

When the power is excited at port ① (Fig. 15), the measured power division S_{21} was -3.34 dB and measured S_{41} was -2.78 dB [see Fig. 16(a)]. Power division characteristics were measured when power was excited at port ③ (Fig. 15); at the design center frequency of 2 GHz measured S_{23} was -2.8 dB

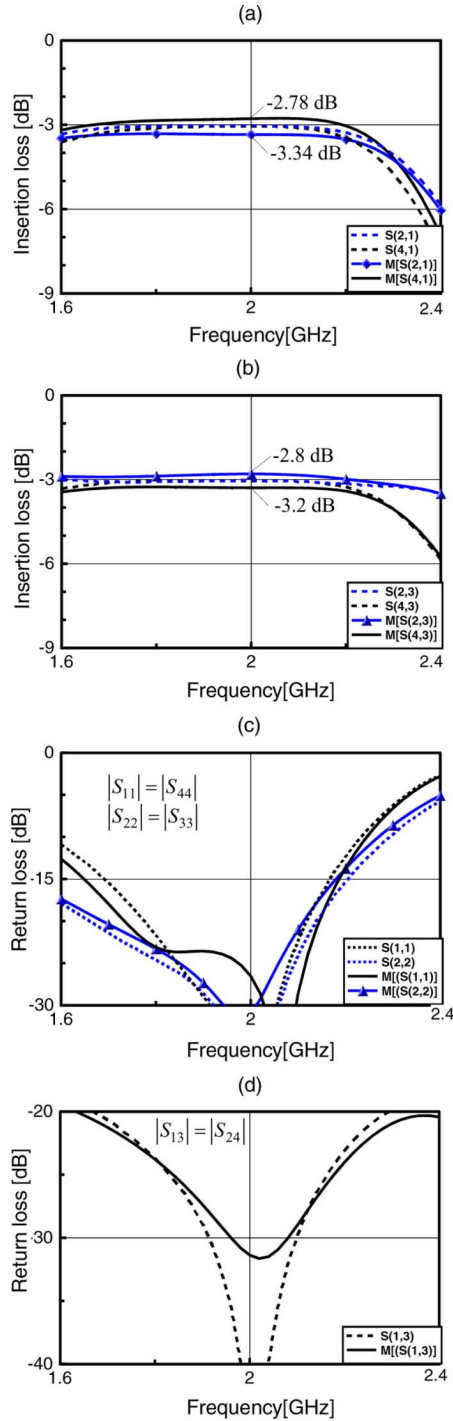


Fig. 16. Results measured and predicted are compared. (a) Power division from port ①. (b) Power division from port ③. (c) Return loss (matching). (d) Isolation.

and measured S_{43} was -3.2 dB [see Fig. 16(b)]. The measured matching performance [see Fig. 16(c)] showed return loss of less than -15 dB in the frequency range of 1.66 – 2.18 GHz. In the proposed SWCLRH, $|S_{11}| = |S_{44}|$, $|S_{22}| = |S_{33}|$, $|S_{13}| = |S_{24}|$, and almost perfect isolation was achieved in more than 20% fractional bandwidth [see Fig. 16(d)]. Considering that simulated values of S_{21} , S_{41} , S_{23} , and S_{43} were about -3 dB, maximum error was about 3%, which seems acceptable and may have been produced by fabrication errors in such parameters as linewidth, line length, and short terminations.

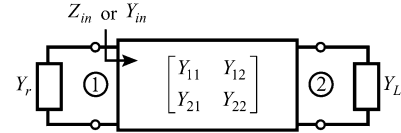


Fig. 17. General two-port circuit.

V. CONCLUSION

In this paper, CLRH and LHRH were discussed and compared. The CLRH was better than the LHRH in all aspects. However, the CLRH had a realization problem in that perfect matching can be achieved only when $C = -3$ dB. To solve this problem, a set of coupled-line sections with two shorts was synthesized and design equations were derived with which the CLRHs could be designed at any of C . Based on the derived design equations, a new modified Π -type transmission-line equivalent circuit was suggested. The modified equivalent circuit was similar to the conventional one, but different in that a set of coupled-line sections was replaced with a transmission-line section. Using the modified transmission-line equivalent circuit, a $3\lambda/4$ transmission-line section of a conventional ring hybrid could be reduced to less than 90° and an SWCLRH was suggested using both modified and conventional transmission-line equivalent circuits. To verify the SWCLRHs, one with a total transmission-line length of 160° was compared with a conventional ring hybrid. Compared to the conventional ring hybrid, the bandwidth of the proposed SWCLRH was much wider than, but was less than, one-third as large.

Using the suggested transmission-line equivalent circuit, the dimensions of all passive components including the ring hybrids can be further reduced. Using the proposed SWCLRHs, all electrical components consisting of ring hybrids can be reduced in size.

APPENDIX

This appendix explains derivation of (3) and (5). A set of coupled-line sections [see Fig. 3(b)] can be equivalent to a general two-port circuit (Fig. 17).

Since the two-port circuit is terminated in arbitrary real admittances Y_r and Y_L , the well-known even- and odd-mode excitation analyses [25] cannot be applied. In the present case, the voltage-based scattering parameters are given as

$$S_{11}^V = -\frac{[(Y_{11} - Y_r)(Y_{22} + Y_L) - Y_{12}Y_{21}]}{\Delta_y} \quad (\text{A1a})$$

$$S_{12}^V = -\frac{1}{\Delta_y} 2Y_L Y_{12} \quad (\text{A1b})$$

$$S_{21}^V = -\frac{1}{\Delta_y} 2Y_r Y_{21} \quad (\text{A1c})$$

$$S_{22}^V = -\frac{[(Y_{11} + Y_r)(Y_{22} - Y_L) - Y_{12}Y_{21}]}{\Delta_y} \quad (\text{A1d})$$

where $\Delta_y = (Y_{11} + Y_r)(Y_{22} + Y_L) + Y_{12}Y_{21}$, $Y_r = 1/Z_r$, and $Y_L = 1/Z_L$.

For the given admittance parameters in (2), Δ_y and numerator N_{11} of S_{11}^V are calculated as

$$\Delta_y = - \left[\left(\frac{Y_{0e} + Y_{0o}}{2} \right)^2 (\cot \Theta)^2 - \left(\frac{Y_{0o} - Y_{0e}}{2} \csc \Theta \right)^2 - Y_r Y_L \right] - j \left(\frac{Y_{0e} + Y_{0o}}{2} \cot \Theta \right) (Y_r + Y_L) \quad (\text{A2a})$$

$$N_{11} = - \left(\frac{Y_{0e} + Y_{0o}}{2} \cot \Theta \right)^2 + \left(\frac{Y_{0o} - Y_{0e}}{2} \csc \Theta \right)^2 - Y_r Y_L - j \left(\frac{Y_{0e} + Y_{0o}}{2} \cot \Theta \right) (Y_L - Y_r). \quad (\text{A2b})$$

The relation between normalized and voltage-based scattering parameters is

$$S_{11} = S_{11}^V \quad (\text{A3a})$$

$$S_{12} = S_{12}^V \sqrt{Y_r/Y_L} \quad (\text{A3b})$$

$$S_{21} = S_{21}^V \sqrt{Y_L/Y_r} \quad (\text{A3c})$$

$$S_{22} = S_{22}^V. \quad (\text{A3c})$$

In (A3), if the termination admittances are equal to each other, then the normalized and voltage-based scattering parameters are identical. Using equations in (A3), the normalized scattering parameters are derived as those in (3).

Terminating port ② of a set of coupled-line sections [see Fig. 3(b)] in Y_L results in a one-port circuit such as a parallel resonance circuit (Fig. 5). In this case, the input admittance Y_{in} is calculated using $Y_{11} - (Y_{12}Y_{21})/(Y_{22} + Y_L)$. The numerator N_{in} and denominator D_{in} of Y_{in} are

$$N_{in} = Y_L A + Y_L \left(\frac{Y_{0e} + Y_{0o}}{2} \cot \Theta \right)^2 + j \left(\frac{Y_{0e} + Y_{0o}}{2} \cot \Theta \right) A - j \left(\frac{Y_{0e} + Y_{0o}}{2} \cot \Theta \right) Y_L^2 \quad (\text{A4a})$$

$$D_{in} = Y_L^2 + \left[\frac{Y_{0e} + Y_{0o}}{2} \cot \Theta \right]^2 \quad (\text{A4b})$$

where

$$A = \left(\frac{Y_{0o} - Y_{0e}}{2} \csc \Theta \right)^2 - \left(\frac{Y_{0e} + Y_{0o}}{2} \cot \Theta \right)^2.$$

The input admittance Y_{in} is equal to that of the parallel resonance circuit (Fig. 5) as

$$\frac{N_{in}}{D_{in}} = \frac{1}{R_o} + j\omega C_o + \frac{1}{j\omega L_o} \quad (\text{A5})$$

Thus,

$$R_o = \frac{Y_L^2 + \left[\frac{Y_{0e} + Y_{0o}}{2} \cot \Theta \right]^2}{Y_L A + Y_L \left(\frac{Y_{0e} + Y_{0o}}{2} \cot \Theta \right)^2} \quad (\text{A6a})$$

$$\omega C_o - \frac{1}{\omega L_o} = \frac{\left(\frac{Y_{0e} + Y_{0o}}{2} \cot \Theta \right) (A - Y_L^2)}{Y_L^2 + \left[\frac{Y_{0e} + Y_{0o}}{2} \cot \Theta \right]^2}. \quad (\text{A6b})$$

Substituting (1) into (A6) gives

$$R_o = \frac{Y_L(1 - C^2) + Y_r \cot^2 \Theta}{Y_r Y_L C^2 \csc^2 \Theta} \quad (\text{A7a})$$

$$\omega C_o - \frac{1}{\omega L_o} = C^2 \frac{\left[\sqrt{\frac{Y_r Y_L}{1 - C^2}} \right]^3 \cot \Theta}{\sin^2 \Theta} - \frac{Y_L \sqrt{Y_r Y_L} \cot \Theta [Y_r \cot^2 \Theta + Y_L(1 - C^2)]}{(\sqrt{1 - C^2})^3}. \quad (\text{A7b})$$

Depending on $\cot \Theta$ in (A7b), capacitance and inductance are computed as those in (5).

REFERENCES

- [1] W. A. Tyrrel, "Hybrid circuits for microwaves," *Proc. IRE*, vol. 35, no. 11, pp. 1294–1306, Nov. 1947.
- [2] V. I. Albanese and W. P. Peyser, "An analysis of a broad-band coaxial hybrid ring," *IRE Trans. Microw. Theory Tech.*, vol. MTT-6, no. 10, pp. 369–373, Oct. 1958.
- [3] W. V. Tyminski and A. E. Hylas, "A wide-band hybrid ring for UHF," *Proc. IRE*, vol. 41, no. 1, pp. 81–87, Jan. 1953.
- [4] S. March, "A wideband stripline hybrid ring," *IEEE Trans. Microw. Theory Tech.*, vol. MTT-16, no. 6, pp. 361–362, Jun. 1968.
- [5] L. K. Yeung and Y. E. Wang, "A novel 180° hybrid using broadside-coupled asymmetric coplanar striplines," *IEEE Trans. Microw. Theory Tech.*, vol. 55, no. 12, pp. 2625–2630, Dec. 2007.
- [6] C.-H. Chi and C.-Y. Chang, "A new class of wideband multisection 180° hybrid rings using vertically installed planar couplers," *IEEE Trans. Microw. Theory Tech.*, vol. 54, no. 6, pp. 2478–2486, Jun. 2006.
- [7] H.-R. Ahn, I. Wolff, and I.-S. Chang, "Arbitrary termination impedances, arbitrary power division and small-sized ring hybrids," *IEEE Trans. Microw. Theory Tech.*, vol. 45, no. 12, pp. 2241–2247, Dec. 1997.
- [8] C.-H. Ho, L. Fan, and K. Chang, "Broad-band uniplanar hybrid-ring and branch-line couplers," *IEEE Trans. Microw. Theory Tech.*, vol. 41, no. 12, pp. 2116–2124, Dec. 1993.
- [9] C.-H. Ho, L. Fan, and K. Chang, "Slotline annular ring elements and their applications to resonator, filter and coupler design," *IEEE Trans. Microw. Theory Tech.*, vol. 41, no. 9, pp. 1648–1650, Sep. 1993.
- [10] C.-H. Ho, L. Fan, and K. Chang, "New uniplanar coplanar waveguide hybrid-ring couplers and magic-T's," *IEEE Trans. Microw. Theory Tech.*, vol. 42, no. 12, pp. 2440–2448, Dec. 1994.
- [11] H. Okabe, C. Caloz, and T. Itoh, "A compact enhanced-bandwidth hybrid ring using an artificial lumped-element left-handed transmission line section," *IEEE Trans. Microw. Theory Tech.*, vol. 52, no. 3, pp. 798–804, Mar. 2004.
- [12] L. Fan, C.-H. Ho, S. Kanamaluru, and K. Chang, "Wide-band reduced-size uniplanar magic-T hybrid ring and de Ronde's CPW-slot couplers," *IEEE Trans. Microw. Theory Tech.*, vol. 43, no. 12, pp. 2749–2758, Dec. 1995.
- [13] M.-H. Murgulescu, E. Moisan, P. Legaud, E. Penard, and I. Zaquine, "New wideband 0.67 λ_g circumference 180° hybrid ring coupler," *Electron. Lett.*, vol. 30, no. 4, pp. 299–300, Feb. 1994.
- [14] T. Hirota, A. Minakawa, and M. Muraguchi, "Reduced-size branch-line and rat-race hybrids for uniplanar MMIC's," *IEEE Trans. Microw. Theory Tech.*, vol. 38, no. 3, pp. 270–275, Mar. 1990.
- [15] M.-L. Chuang, "Miniaturized ring coupler of arbitrary reduced size," *IEEE Microw. Wireless Compon. Lett.*, vol. 15, no. 1, pp. 16–18, Jan. 2005.
- [16] H.-R. Ahn, *Asymmetric Passive Components in Microwave Integrated Circuits*. New York: Wiley, 2006, p. 78.
- [17] H.-R. Ahn, I.-S. Chang, and S.-W. Yun, "Miniaturized 3-dB ring hybrid terminated by arbitrary impedances," *IEEE Trans. Microw. Theory Tech.*, vol. 42, no. 12, pp. 2216–2241, Dec. 1994.

- [18] S. J. Parisi, "180° lumped element hybrid," in *IEEE MTT-S Int. Microw. Symp. Dig.*, 1989, pp. 1243–1246.
- [19] R. K. Gupta and W. J. Gestinger, "Quasi-lumped-element 3- and 4-port networks for MIC and MMIC applications," in *IEEE MTT-S Int. Microw. Symp. Dig.*, 1984, pp. 409–411.
- [20] H.-R. Ahn and B. Kim, "Transmission-line directional couplers for impedance transforming," *IEEE Microw. Wireless Compon. Lett.*, vol. 16, no. 10, pp. 537–539, Oct. 2006.
- [21] H.-R. Ahn and B. Kim, "Toward integrated circuit size reduction," *IEEE Microw. Mag.*, pp. 65–75, Feb. 2008.
- [22] H.-R. Ahn, *Resonators Encyclopedia of RF and Microwave Engineering*. New York: Wiley, 2005.
- [23] G. Mathaei, L. Young, and E. M. T. Jones, *Microwave Filters, Impedance-Matching Networks and Coupling Structures*. Norwood, MA: Artech House, 1985, pp. 36–.
- [24] Y. Konishi, I. Awai, Y. Fukuoka, and M. Nakajima, "A directional coupler of a vertically installed planar circuit structure," *IEEE Trans. Microw. Theory Tech.*, vol. 36, no. 6, pp. 1057–1063, Jun. 1988.
- [25] J. Reed and G. J. Wheeler, "A method of analysis of symmetrical four-port networks," *IEEE Trans. Microw. Theory Tech.*, vol. MTT-4, no. 10, pp. 346–352, Oct. 1956.



Hee-Ran Ahn (S'90–M'95–SM'99) received the B.S., M.S., and Ph.D. degrees in electronic engineering from Sogang University, Seoul, Korea, in 1988, 1990 and 1994, respectively.

From 1991 to 1995, she was a Part-Time Lecturer with Sogang University. From 1996 to 1997, she was a Post-Doctoral Fellow with Duisburg–Essen University, Duisburg, Germany. From February 1997 to 2002, she was with the Department of Electrical Engineering, Duisburg–Essen University, where she was involved with habilitation dealing

with asymmetric passive components in microwave circuits. She is currently with the Department of Electronics and Electrical Engineering, Pohang Uni-

versity of Science and Technology (POSTECH), Pohang, Gyungbuk, Korea. From March 2003 to February 2005, she was with the Division of Electrical Engineering, Department of Electrical Engineering and Computer Science, Korea Advanced Institute of Science and Technology (KAIST), Daejeon, Korea, as a Visiting Professor. She authored *Asymmetric passive component in microwave integrated circuits* (Wiley, 2006). Her research interests include high-frequency and microwave circuit design and biomedical applications using microwave theory and techniques.



Bumman Kim (S'77–M'78–SM'97–F'07) received the Ph.D. degree in electrical engineering from Carnegie Mellon University, Pittsburgh, PA, in 1979.

From 1978 to 1981, he was engaged in fiber-optic network component research with GTE Laboratories Inc. In 1981, he joined the Central Research Laboratories, Texas Instruments Incorporated, where he was involved in development of GaAs power field-effect transistors (FETs) and monolithic microwave integrated circuits (MMICs). He has developed a large-signal model of a power FET, dual-gate FETs for gain control, high-power distributed amplifiers, and various millimeter-wave monolithic microwave integrated circuits (MMICs). In 1989, he joined the Pohang University of Science and Technology (POSTECH), Pohang, Gyungbuk, Korea, where he is a Namko Professor with the Department of Electrical Engineering, and Director of the Microwave Application Research Center, where he is involved in device and circuit technology for RF integrated circuits (RFICs). In 2001, he was a Visiting Professor of electrical engineering with the California Institute of Technology, Pasadena. He has authored over 200 technical papers.

Dr. Kim is a member of the Korean Academy of Science and Technology and the Academy of Engineering of Korea. He was an associate editor for the *IEEE TRANSACTIONS ON MICROWAVE THEORY AND TECHNIQUES*. He is a Distinguished Lecturer of the IEEE Microwave Theory and Techniques Society (IEEE MTT-S).